Near-infrared adaptive optics imaging
of the satellites and individual rings of Uranus ☆

S.G. Gibbard [a,*], I. de Pater [b], H.B. Hammel [c]

[a] *Lawrence Livermore National Laboratory, Livermore, CA 94550, USA*
[b] *Astronomy Department, 601 Campbell Hall, University of California, Berkeley, CA 94720, USA*
[c] *Space Science Institute, 4750 Walnut Street, Suite 205, Boulder, CO 80301, USA*

Abstract

We present the first Earth-based images of several of the individual faint rings of Uranus, as observed with the adaptive optics system on the W.M. Keck II telescope on four consecutive days in October 2003. We derive reflectivities based on multiple measurements of 8 minor moons of Uranus as well as Ariel and Miranda in filters centered at wavelengths of 1.25(J), 1.63(H), and 2.1(Kp) μm. These observations have a phase angle of $1.84°$–$1.96°$. We find that the small satellites are somewhat less bright than in observations made by the HST at smaller phase angles, confirming an opposition surge effect. We calculate albedoes for the ring groups and for each ring separately. We find that the ϵ ring particles, as well as the particles in the three other ring groups, have albedoes near 0.043 at these phase angles. The equivalent depths of some of the individual rings are different than predicted based upon ring widths from occultation measurements (assuming a constant particle ring brightness); in particular the γ ring is fainter and the η ring brighter than expected. Our results indicate that q, the ratio of ϵ ring intensity at apoapse vs. periapse, is close to 3.2 ± 0.16. This agrees well with a model that has a filling factor for the ϵ ring of 0.06 (Karkoschka, 2001, Icarus 151, 78–83). We also determine values of the north to south brightness ratio for the individual rings and find that in most cases they are close to unity.

© 2004 Elsevier Inc. All rights reserved.

Keywords: Uranus; Planetary rings, Uranus; Infrared observations

1. Introduction

Observations of the uranian system, both from the Earth and from the Voyager 2 spacecraft in 1986 (Smith et al., 1986; Stone and Miner, 1986), have revealed a number of satellites as well as an extensive ring system. The Uranus ring system consists of groups of narrow annuli in the planet's equatorial plane, interior to $\sim 2R_U$. The outermost ϵ ring ranges in width from 20 km at periapse to 96 km at apoapse. There are three other ring groups interior to the ϵ ring, consisting of narrow rings with widths between 2 and 12 km. The shepherding moons Cordelia and Ophelia confine the ϵ ring (Porco and Goldreich, 1987), and other undetected shepherd moons may confine the other rings. Voyager observations, in combination with stellar occultation data, indicate that the rings consist of primarily > cm size particles (French et al., 1991). Their spectra are flat at visible and near-infrared wavelengths, and their albedoes are quite low.

The small angular separation between Uranus and its rings (42,000 km, < 4″), as well as between the rings themselves (⩽ 2700 km or 0.2″ between groups, ⩽ 1000 km or 0.08″ between individual rings) makes it difficult to discern details of the ring structure from ground-based telescopes. Uranus' faint rings and close moons are difficult to detect at visible wavelengths due to scattered light from the planet,

* Corresponding author.
E-mail address: sgibbard@igpp.ucllnl.org (S.G. Gibbard).

but can be more easily observed at wavelengths near 2 μm, where the planet appears dark due to strong methane absorption. Baines et al. (1998) and Sromovsky et al. (2000) published ground-based images of Uranus and its rings in which the ϵ ring with its asymmetric brightness distribution was easily observed, but due to the relatively low spatial resolution (typically $\sim 0.5''$ from the ground) none of the other rings could be seen. Karkoschka (2001a) published photometry of the uranian moons and ring system from Hubble Space Telescope images, including the ϵ ring and the three inner ring groups at visible to near-infrared wavelengths.

de Pater et al. (2002) presented Keck adaptive optics (AO) observations of the uranian system, which were taken soon after the AO system became a facility instrument. Since their field of view was $4.5''$, they mosaicked Uranus to form a complete picture of the planet and its rings. Their images clearly revealed the ϵ ring and the three inner ring groups. During their observations, the observers noted that extended objects can introduce artifacts in an AO system with a quad-cell Shack–Hartmann sensor, as described in detail in their paper. In response to this, the Keck AO team implemented a procedure which optimizes the AO system for extended objects (van Dam and Macintosh, 2003; van Dam et al., 2004).

We report here on observations of Uranus from Keck in October 2003, which show that use of the newly-optimized AO system led to greatly improved Strehl ratios, and hence better image quality. During these observations we achieved a Strehl ratio of 0.5 and a spatial resolution of $\leqslant 0.05''$. This is sufficient to resolve (for the first time from an Earth-based image) individual annuli including the α, β, γ, η, and δ rings. We present photometry of the individual uranian rings, as well as the satellites Miranda, Ariel, and eight smaller moons, and compare our findings to the results of Karkoschka (2001a) and de Pater et al. (2002).

2. Observations

We observed Uranus with the 10-m W.M. Keck II telescope[1] on Mauna Kea, Hawaii, on October 3–6 2003 (UT). Images were obtained using the NIRC2 camera, a 1024×1024 Aladdin-3 InSb array.[2] We obtained a typical spatial resolution of 0.043–0.051 arcsec on nearby stars (which corresponds to about 700 km at Uranus) at all wavelengths observed. Our ring observations are summarized in Table 1; characteristics of the filters are shown in Table 2.

Table 1
Uranus ring observations

Date (UT)	Time (UT)	Wavelength	Exposure time (s)	FWHM
5 Oct 2003	9:06	Kp	300	0.051
5 Oct 2003	9:33	J	180	0.045
5 Oct 2003	9:38	H	300	0.043
6 Oct 2003	5:35	J	180	0.049
6 Oct 2003	9:07	Kp	300	0.045
6 Oct 2003	9:33	H	300	0.045

Table 2
Filter characteristics

Filter name	Central wavelength (μm)	Wavelength range (μm)
J	1.25	1.17–1.33
H	1.63	1.48–1.78
Kp	2.12	1.95–2.30

Filter traces and further information are available at: http://alamoana.keck.hawaii.edu/inst/nirc2/filters.html.
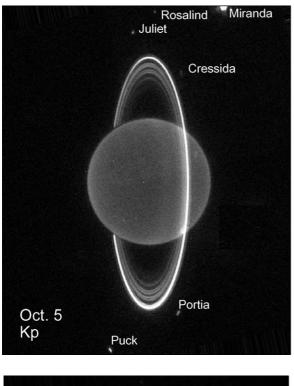
The images were reduced using standard infrared techniques: they were flatfielded using twilight and dome flats, bad pixels were removed (replaced with the median of neighboring pixels), and the sky was subtracted using a separate image of the sky taken just prior or after the Uranus exposure itself. Figure 1 shows images of the Uranus system for October 5 and 6 2003. On these dates we took single long exposures (600 s) of the uranian ring system, which produced the clearest ring separation of any of our images. These were the images used for the modeling of the ring system (discussed below). Since the disk of Uranus decreases in brightness from J to Kp due to strong methane absorption at Kp, and the ring reflectivities do not vary much with wavelength, the rings are more easily seen at Kp band. Several of the uranian moons are also visible, particularly at Kp band (labeled in Fig. 1). The ϵ ring is easily separated from the other rings within our resolution; the three rings groups are also clearly resolved. The α and β rings are just resolved at a separation of $0.07''$, and the δ, η, and γ rings are also resolved at separations of $0.06''$ and $0.10''$. The 456 rings, although clearly extended, are unresolved. Numerous bright features are visible on the disk of Uranus near the South Polar bright band and at high northern latitudes, as previously reported by Karkoschka (1998) and Hammel et al. (2001). There are also features near the equator, at latitudes where such activity has never been detected before. The dynamics and wind velocity profiles of these features are the subject of a paper by Hammel et al. (2004).
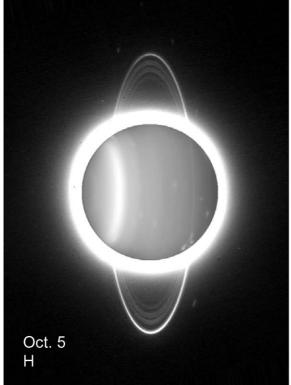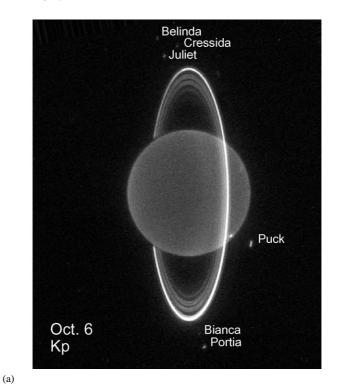
3. Satellite photometry

Photometry of adaptive optics images requires an assessment of the amount of light from the observed object that is concentrated in the centermost $0.3''$ (the approximate radius of control for the Keck adaptive optics system) and the residual light that is spread into a 'halo' that extends out to an arc-

---

[1] The Keck telescope is jointly owned and operated by the University of California and the California Institute of Technology.

[2] Designed by Keith Matthews and Tom Soifer, both of Caltech. The instrument was built by Keith Matthews and engineer Sean Lin of Caltech, with help from James Larkin, Ian McLean, and others at UCLA (detector electronics and related software), and Al Conrad, Bob Goodrich, and Allan Honey at Keck Observatory (software). Support in Waimea was provided by Jim Bell, Randy Campbell, and Drew Medeiros.
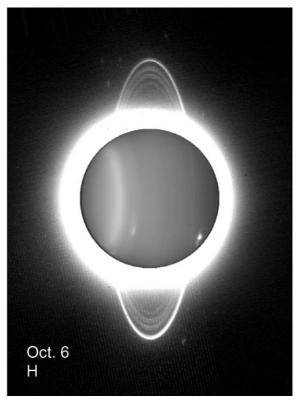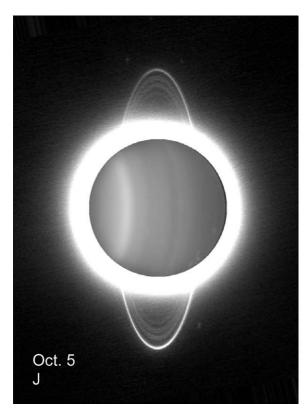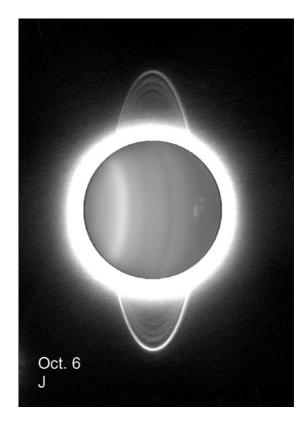
(a)

(b)

Fig. 1. Images of Uranus taken on 5 and 6 October 2003 (UT) in three near-infrared broadband filters. The Kp (2.1 μm) images are shown unaltered; in the J (1.25) and H (1.63) band images the planet's intensity (out to its physical radius) has been reduced by a factor of 30 so that the rings and details of the planet's disk can be shown in the same image. Scattered light from the planet is important at J and H band, but at Kp band methane absorption sharply reduces the light from the planet so that details of the ring structure and the satellites (labeled in the images) can be seen.

second or more. In a crowded field with considerable scattered light from Uranus, it is important to use a small photometric aperture, while at the same time accounting for the missing flux from the object. In order to do this, we used a 'bootstrap' procedure as follows: a photometric standard star was observed in "open loop" (non-AO) mode (this star was

(c)

Fig. 1. Continued.

too bright to be observed in AO mode) and the total counts for the star were calculated. This was used for the conversion of data counts to actual flux. We also observed a point spread function (PSF) star in AO mode. Using apertures of $1.5''$ (which contains essentially all the flux from the PSF) and $0.5''$ we calculated the ratio of the total flux from the PSF to the ratio contained within $0.5''$ (for our data this ratio was 1.2). For photometry of the large satellites of Uranus (Ariel and Miranda), we determined the number of counts within an aperture of $0.5''$, then multiplied this by the factor 1.2 to get the total counts. We then used variable apertures on Ariel and Miranda ranging from 0.15 to $0.5''$, and calculated the ratio of the fraction of light within the smaller apertures to the ratio at $0.5''$. This provided us the conversion factor for counts on the smaller moons at the decreased aperture size. This ratio was found to be fairly consistent from image to image for a small aperture size of 0.20 arcsec (ratio of 1.5 for an aperture of $0.5''$ vs. $0.2''$). We therefore used this aperture size and ratio for the other satellites of Uranus. In cases where the brighter satellites Puck and Portia were located close to the planet and there was considerable scattered light, we estimated the contribution of the scattered light using an aperture of the same size in an area that had a similar background flux (this was necessary for some satellites at H and J band, but not at Kp where scattered light from the planet is minimal). For the fainter satellites we did not attempt to calculate a brightness for satellites close to the planet.

Satellite integrated I/F values are given in Table 3. In order to convert our I/F numbers to satellite reflectivities we multiplied by the ratio of the area of a single pixel (here 10^{-4} arcsec^2 or 16,900 km^2) to the area of the satellite. We assumed that each satellite had the average cross-section given in Karkoschka (2001a, 2001b). We have searched for evidence of variation in satellite brightness due to the different orbital phase and therefore different cross-section of the satellites. Several of the satellites (most notably Juliet and Belinda) are believed to have an oblong shape which could lead to different integrated I/F when viewed at different phases of their orbits. Although we did not detect any such variation, our observations of Juliet were only near the northern ring ansa, and for Belinda near the northern and southern ansae. In cases where the satellites were closer to Uranus we were not able to determine reflectivity due to scattered light from the planet. Therefore we were unlikely to see a significant variation in I/F due to a change in cross-section.

Table 4 gives averages and error estimates for the reflectivities of the satellites based on the assumptions made above. In cases where satellites were observed at least three times at a given wavelength, the errors bars were constructed from the standard deviation of the measurements, added in quadrature to the estimated photometric error (5%). For satellites with only one or two observations at a given wavelength, errors were estimated as the sum in quadrature of the photometric error and the estimated noise. Noise was estimated for each image as the average of the noise in apertures at intervals of 20° at a distance of $1''$ from the planet. Separate estimates were made using apertures of size $0.2''$ and $0.5''$. The noise estimate for the larger aperture was used for

Table 3
Moon integrated I/F

Date (UT)	λ	Phase	Ariel	Miranda	Puck	Portia	Juliet	Cressida	Belinda	Rosalind	Desdemona	Bianca
Oct. 3 5:44	J	1.84	–	2.07	–	0.043	–	–	0.010	–	–	–
Oct. 3 9:09	J	1.85	–	–	–	–	0.026	–	–	–	–	–
Oct. 4 5:18	J	1.88	–	–	0.075	–	–	–	0.019	–	–	–
Oct. 4 7:20	J	1.88	–	–	–	0.032	–	–	–	–	–	–
Oct. 4 9:55	J	1.89	–	–	0.063	–	0.017	–	0.021	–	–	–
Oct. 5 5:18	J	1.92	–	2.14	0.063	–	–	–	–	–	–	–
Oct. 5 7:20	J	1.92	–	2.29	0.066	0.030	0.026	–	–	–	–	–
Oct. 5 9:33	J	1.92	–	–	–	0.033	0.021	0.008	–	0.012	–	–
Oct. 6 5:35	J	1.95	17.4	–	–	–	–	–	–	–	–	–
Oct. 6 6:56	J	1.96	–	–	–	0.036	0.020	–	0.016	–	–	–
Oct. 3 5:22	H	1.84	–	1.66	–	0.037	–	–	0.020	–	–	–
Oct. 3 9:32	H	1.85	–	–	–	–	0.020	–	–	0.010	–	–
Oct. 4 5:03	H	1.88	–	–	0.072	–	–	–	0.011	0.011	–	–
Oct. 4 7:03	H	1.88	–	–	0.077	0.038	0.020	–	0.013	–	–	–
Oct. 4 9:39	H	1.89	–	–	–	0.027	0.025	–	0.016	–	–	0.0078
Oct. 5 5:02	H	1.92	–	1.78	0.078	–	–	–	–	–	–	–
Oct. 5 7:00	H	1.92	–	1.81	0.078	0.038	–	–	0.013	–	–	0.0034
Oct. 5 9:17	H	1.92	–	–	–	0.029	0.022	0.0088	–	0.010	–	–
Oct. 6 5:20	H	1.96	13.3	–	–	–	–	–	–	0.015	0.018	–
Oct. 6 7:11	H	1.96	–	–	0.083	–	0.021	0.0057	–	–	–	–
Oct. 6 9:47	H	1.96	–	–	–	0.031	0.016	–	0.011	–	–	–
Oct. 3 5:53	Kp	1.84	–	1.50	–	0.052	–	–	0.016	0.012	–	–
Oct. 3 9:40	Kp	1.85	–	–	0.072	–	0.032	–	–	–	–	0.012
Oct. 4 5:24	Kp	1.88	–	–	0.069	0.045	–	0.017	0.017	0.012	0.017	–
Oct. 4 7:28	Kp	1.88	–	–	–	0.047	0.032	0.016	–	0.015	0.019	–
Oct. 4 10:01	Kp	1.89	–	–	0.085	–	0.027	–	0.017	–	–	0.016
Oct. 5 5:22	Kp	1.92	–	1.55	0.076	–	–	–	–	–	–	–
Oct. 5 7:28	Kp	1.92	–	1.60	0.070	0.045	0.031	–	0.010	–	–	–
Oct. 5 9:06	Kp	1.92	–	1.45	0.070	0.043	–	0.011	–	0.018	–	–
Oct. 6 5:40	Kp	1.95	12.25	–	–	–	–	–	0.014	0.0094	–	–
Oct. 6 7:17	Kp	1.96	–	–	0.078	0.054	0.038	0.017	–	–	–	–
Oct. 6 9:07	Kp	1.96	–	–	0.081	0.047	0.031	0.018	0.013	–	0.013	–

Ariel and Miranda, while the estimate for the smaller aperture was used for the other satellites.

Since our observations were made at a phase angle of 1.84°–1.96°, they are complementary to the low phase angle measurements (< 0.1°) made at these wavelengths by Karkoschka (2001a). Karkoschka found the brightness of the satellites to be higher at phase angles near 0°, which indicates an "opposition surge." In combination with Karkoschka's data, our results confirm the decrease in reflectivity at larger phase angles. We find that the reflectivities of the large satellites Ariel and Miranda are not constant across wavelength, but instead show a decrease from J band to Kp. The decreased flux of the larger uranian satellites at Kp has previously been attributed to water ice (Brown and Cruikshank, 1983). A marginal detection of water ice on Puck was made by Karkoschka (2001a), based on a dip in its spectrum at 2.03 μm. Within error bars we do not observe this effect in our broadband filters for any of the small satellites we observed.

The uranian rings show very little if any measurable color variation across this wavelength range (see Section 4 below), indicating an absence of exposed water ice on the surface of the ring particles. The reflectivity of the planet itself (Fig. 2,
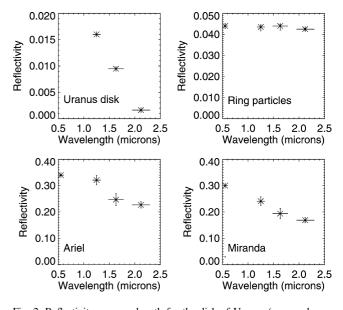

Fig. 2. Reflectivity vs. wavelength for the disk of Uranus (averaged over 5 and 6 October), ring particles, Miranda, and Ariel. Near-infrared values are from this work; the horizontal bars represent the wavelength range of the broadband filters. Values at 0.55 μm are extrapolated from Karkoschka (2001a, Fig. 6) to values expected for a phase angle of 1.9°.

Table 4
Average Uranus moon reflectivities in the near-IR

Wavelength	Ariel	Miranda	Puck	Portia	Juliet	Cressida	Belinda	Rosalind	Desdemona	Bianca
J (1.25 µm)	0.321 ± 0.018[a]	0.241 ± 0.017	0.064 ± 0.0064	0.044 ± 0.0082	0.049 ± 0.010	0.029 ± 0.016[a]	0.050 ± 0.018	0.058 ± 0.008[a]	–	–
H (1.63 µm)	0.247 ± 0.023[a]	0.194 ± 0.020	0.074 ± 0.014	0.042 ± 0.0071	0.047 ± 0.021	0.027 ± 0.015[a]	0.043 ± 0.020	0.055 ± 0.017	–	0.047 ± 0.05[a]
Kp (2.12 µm)	0.227 ± 0.012[a]	0.169 ± 0.010	0.072 ± 0.0056	0.060 ± 0.0072	0.071 ± 0.011	0.058 ± 0.013	0.044 ± 0.0070	0.064 ± 0.014	0.08 ± 0.021	0.12 ± 0.05[a]

[a] 1-σ error based on estimated noise and photometry error; all others are photometry error plus standard deviation of multiple observations.

first panel) is a strongly decreasing function of wavelength. Our values for the disk reflectivity (0.016 at J, 0.0095 at H, and 0.00016 at Kp) agree very well with those found by de Pater et al. (2002) (0.015 at J, 0.0090 at H, and 0.00016 at Kp).

4. Rings

4.1. Ring particle reflectivities

Determining the amount of light that comes from each of the rings is complicated by the effects of the non-symmetric and time-varying PSF and the light scattered from the planet and the bright ϵ ring. In order to account for these effects we constructed a model of the planet and ring system. This consisted of a (spherical) planet with constant brightness[3] (equal to the average I/F of Uranus), and the nine rings: ϵ, δ, γ, η, β, α, 4, 5, and 6. Each ring was represented as a single-pixel-wide ellipse at its appropriate distance from Uranus. Since most pixels have only a fraction of the ellipse passing through them, we assigned to each pixel a value equal to the fraction of the ellipse that occupies it. Each ring was then assigned a brightness that could be varied to get the best fit to the data. Another free parameter was the azimuthal gradient in brightness in the ϵ ring. The other rings were assumed to be azimuthally invariant; this assumption was tested as described below in Section 4.2. The ring + planet model (the planet is important here as a source of scattered light) was then convolved with the PSF of a reference star at the appropriate wavelength.

The best fit parameter we chose to compare our model to was an average 'slice' of the data constructed by deprojecting the data on a radius-longitude grid and averaging across the ring system. The actual comparison was made to the difference between the data and a 30-pixel smoothed image, which helps to remove the effects of scattered light. The same procedure was applied to the ring model. Since the effects of scattered light from the ϵ ring are minimized at periapse, the slice was constructed using an average projection of $\pm 5°$ from the northern and southern ansae of the rings. This model slice was compared to the data slice and the values of all ten model parameters were varied (using the downhill simplex method described in Press et al., 1992) until a best fit was reached. The procedure was similar to that used in de Pater et al. (2002). Comparisons of the data and model slices are shown in Figs. 3a–3d. The model values for ring I/F are given in Table 5.

In order to convert the ring I/F in our model into actual ring particle brightnesses, we considered the visible area of

---

[3] Due to the smoothing and subtracting procedure discussed below, the results are quite insensitive to the shape of the planet or the value of the planet's, reflectivity; for example, a change in the planet's I/F of 100% produces a $< 1\%$ change in the ring brightness, small compared to the error in the observations.
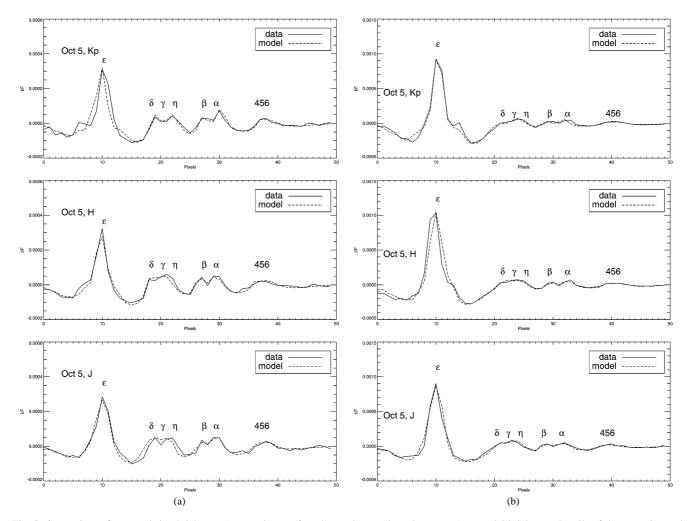
Fig. 3. Comparison of averaged ring brightness (averaged over 5° at the northern and southern ansae) to model brightness. Details of the averaging and modeling procedure are discussed in the text. (a) Data from 5 October, northern ansa. (b) 5 October, southern ansa. (c) 6 October, northern ansa. (d) 6 October, southern ansa.

Table 5
Uranus rings modeled I/F

Ring	Wavelength	J	H	K
North				
ϵ		4.1×10^{-3}	4.1×10^{-3}	4.0×10^{-3}
δ		1.4×10^{-3}	1.2×10^{-3}	1.0×10^{-3}
γ		5.7×10^{-4}	7.3×10^{-4}	4.5×10^{-4}
η		1.1×10^{-3}	8.0×10^{-4}	9.5×10^{-4}
β		1.2×10^{-3}	1.1×10^{-3}	1.5×10^{-3}
α		1.2×10^{-3}	9.6×10^{-4}	1.3×10^{-3}
4		4.3×10^{-4}	4.9×10^{-4}	4.7×10^{-4}
5		2.0×10^{-4}	7.9×10^{-5}	2.1×10^{-4}
6		3.7×10^{-4}	3.3×10^{-4}	3.0×10^{-4}
South				
ϵ		1.3×10^{-2}	1.2×10^{-2}	1.3×10^{-2}
δ		1.6×10^{-3}	1.2×10^{-3}	8.5×10^{-4}
γ		9.0×10^{-4}	6.1×10^{-4}	4.4×10^{-4}
η		1.6×10^{-3}	1.0×10^{-3}	1.1×10^{-3}
β		1.2×10^{-3}	1.1×10^{-3}	1.0×10^{-3}
α		1.2×10^{-3}	1.2×10^{-3}	1.0×10^{-3}
4		3.2×10^{-4}	3.8×10^{-4}	3.5×10^{-4}
5		1.7×10^{-4}	8.2×10^{-5}	1.8×10^{-4}
6		3.7×10^{-4}	1.8×10^{-4}	3.5×10^{-4}

the rings. The area of the rings that is visible at a given time is a function of the subsolar latitude and the phase angle of observation. Karkoschka (2001b, Fig. 6) gives fractional visible areas for the rings of Uranus. For our observations at a sub-Earth latitude of 18.8°–19.6°, the visible fractions are approximately: 0.3 for the ϵ ring; 0.55 for $\alpha\beta$; 0.5 for $\eta\gamma\delta$; and 0.65 for 456. Multiplying these factors by the areas given in Table 1 of Karkoschka (2001b), which are based on equivalent depths from French et al. (1986), gives the visible ring areas. We then construct a particle reflectivity by multiplying the modeled ring I/F by the ratio of the modeled ring area to the actual visible area.

Table 6 shows the average ring particle reflectivities derived from the modeled I/F given in Table 5. Since we found no significant difference in ring albedo at the wavelengths we observed, these values are based on an average of the J, H, and K measurements. The ratio of the brightness of the rings at the southern vs. the northern ansa is also shown in Table 6.

Our reflectivities for the ϵ ring particles and for the particles of the three ring groups (ϵ ring = 0.043, $\eta\gamma\delta$ = 0.041,
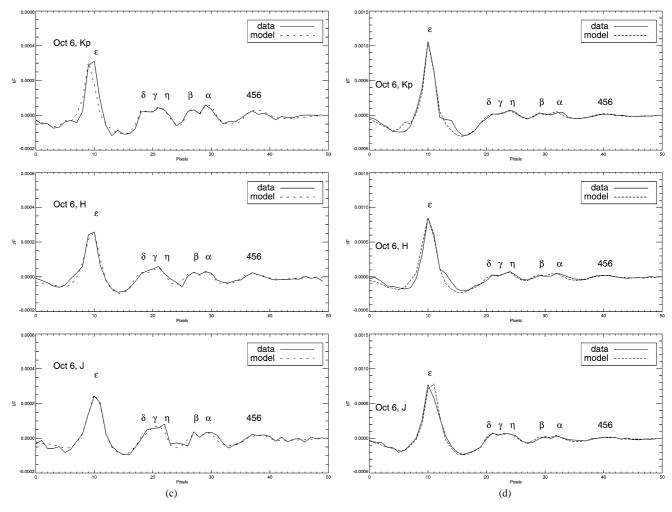
Fig. 3. Continued.

Table 6
Average ring particle reflectivities

Ring (group)	Reflectivity	A (km)	A' (km)	South/north ratio
ϵ	0.043 ± 0.002	95.0	95.0	3.2 ± 0.16
$\delta + \delta_c$	0.050 ± 0.008	4.99	5.69 ± 0.91	1.03 ± 0.21
γ	0.019 ± 0.004	6.57	3.67 ± 0.77	1.07 ± 0.29
$\eta + \eta_c$	0.081 ± 0.016	2.52	3.70 ± 0.74	1.26 ± 0.21
$\delta\gamma\eta$	0.041 ± 0.005	14.08	13.45 ± 1.64	–
β	0.051 ± 0.004	6.68	7.73 ± 0.60	1.0 ± 0.04
α	0.033 ± 0.004	4.27	3.47 ± 0.42	1.0 ± 0.18
$\alpha\beta$	0.044 ± 0.003	10.95	11.2 ± 0.76	–
4	0.053 ± 0.014	1.41	1.58 ± 0.42	0.78 ± 0.19
5	0.017 ± 0.004	1.81	2.44 ± 0.57	0.92 ± 0.11
6	0.065 ± 0.018	0.82	0.61 ± 0.17	1.03 ± 0.30
456	0.039 ± 0.006	4.04	3.71 ± 0.57	–

Note: A = equivalent depth (from French et al., 1986); A' = equivalent depth assuming that all rings have the ϵ ring particle reflectivity.

$\alpha\beta = 0.044$, $456 = 0.039$) can be compared to values reported by previous observers. Since the rings appear to be gray (this paper, Fig. 2, Karkoschka, 2001a; de Pater et al., 2002), we will compare values without reference to specific wavelengths, considering only the effects of different phase angles. Karkoschka (2001a) found reflectivities of be-

tween 0.04 and 0.05 at phase angles of 0.03° to 3°, while Voyager data at larger phase angles indicated a much lower reflectivity of 0.02. Figure 6 from Karkoschka, 2001a indicates that, according to his model of the variation of the ring brightness with phase angle, at a phase angle of 2° the ring particle reflectivity should be 0.044. The values we find for the ϵ ring and the three ring groups are in good agreement with this. de Pater et al. (2002) reported the following H-band reflectivities at a phase angle of 2.82°: ϵ ring $= 0.042$, $\eta\gamma\delta = 0.042$, $\alpha\beta = 0.041$, $456 = 0.033$. These values are in excellent agreement with our observations. Both our observations and those of de Pater et al. suggest that the 456 ring group may have a somewhat lower particle reflectivity than the others, although this finding does not reach the level of statistical significance.

We have also determined the particle brightness of the individual rings (Table 6). Using the equivalent depth values given by French et al. (1986), the results that we find for the individual rings are quite variable (although by averaging over ring groups we find values that are quite close to the value for the ϵ ring). These variations in brightness between the individual rings include a lowered value of the γ ring and an increase in the η ring. A smaller discrepancy is also
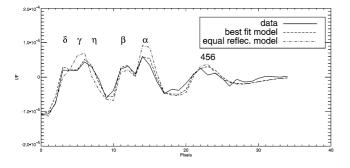
Fig. 4. Comparison of averaged ring brightness on October 6 at Kp to two models. The first model is the best-fit model shown in Fig. 3; the second is a model in which the individual rings are assumed to all have the same ring particle brightness, equal to the average ring brightness of the ring group. Equivalent depths from French et al. (1986) have been assumed to calculate the ring particle brightness.

Table 7
Ring pericenters

Ring	Oct. 3 5:22 UT	Oct. 6 9:47 UT
ϵ	121.3	125.7
δ	–	–
γ	198.1	203.7
η	–	–
β	128.3	134.7
α	299.6	306.6
4	135.0	143.3
5	169.8	178.3
6	35.9	44.7

found for α and β rings, the β ring being brighter than expected and α somewhat fainter. The 5 ring also has a greatly decreased brightness compared to the 4 and 6 rings, but we do not consider this to be significant, as these rings are not resolved.

If we make the assumption that all the ring particles have the same albedo as the ϵ ring, then some of the ring equivalent depths are considerably different than those given by French et al. (1986). Table 6 gives values for the equivalent depths of the rings based on the assumption that all rings have the ϵ reflectivity of 0.043. We again assume the fractional visible areas given by Karkoschka (2001b). Figure 4 shows a comparison of the best-fit Kp model for October 6 and a model that assumes all the rings have an albedo equal to their ring group averages. From this it can be seen that the equal-reflectivity model is not a good fit for either the $\delta\gamma\eta$ group or the $\alpha\beta$ group, although for the unresolved 456 group there is little difference in the best-fit and the equal reflectivity models. Therefore it seems that either the individual rings do not have the ring group averages (which we consider to be less likely), or that the visible ring areas or equivalent depths are not correct. Given the uncertainty inherent in trying to derive the albedo of particles in an optically-thick ring (Dones et al., 1993), as well as the uncertainly in our modeling, it is perhaps not surprising that our results for the individual rings show a discrepancy with previous models. Further observations at different ring opening angles may improve our understanding of the ring particle albedo.

4.2. Ring brightness as a function of orbital phase

The ϵ ring exhibits a large variation in width, ranging from 96 km at apoapse to only 20 km at periapse. Because the optical depth of the ring is greater than 1 at periapse and less than 1 at apoapse, the ratio of the brightness at apoapse to the brightness at periapse, q, is not merely the ratio of the ring widths. The value of q is important as a diagnostic of the "filling factor" D, the fractional volume of the ring occupied by ring particles. Determining the value of D from the observed q requires a model of the ring particles; the model

used by many observers is that of Hapke (1981). However, Karkoschka (2001b) used a model by Irvine (1966) that better accounts for the observed increase in brightness caused by reduced ring particle shadowing at opposition. Using this model he predicts that the ratio q will increase from 2 to 5 as Uranus approaches ring plane crossing in 2007.

Svitek and Danielson (1987) found values of q near 2.4 for Voyager 2 observations. Karkoschka (2001b) gives values of $q \simeq 2.5$ for HST measurements at phase angles between 0.03 and 3. Combining these data with a Voyager measurement at a phase angle of 20° (at larger phase angles q is highly diagnostic of the filling factor D) Karkoschka concludes that a value of $D = 0.06$ is the best fit to all the data. If we use Karkoschka's result with $D = 0.06$, we would expect $q = 3.2$ for our data at a sub-Earth latitude of $-18.9°$ (Karkoschka, 2001b, Fig. 5). In an analysis of six ring images (Table 5), two each at J, H, and Kp, we find the average value of the south to north ratio to be 3.2 ± 0.16, in excellent agreement with Karkoschka's prediction. We note that the north/south ratio is not exactly the same as q, since the periapsis of the ϵ ring was not located exactly at the northernmost edge of the rings (Table 7); therefore the actual value of q may be somewhat larger than this.

The brightness ratios of the other rings may also vary as a function of ring width, which for some of the rings may be a simple function of longitude. For example, the ϵ, α, β, and δ rings show a simple correlation between the width and orbital phase, with a maximum width occurring near apoapsis (French et al., 1991). The gamma ring also shows width variations, but there is no obvious relation to the orbital phase. In our model we varied the brightness of the ϵ ring with orbital phase, but considered the other rings to be of equal brightness at all phases. To test the validity of this assumption we also modeled the data at the southern ansa. As Table 7 shows, at the time of our observations the periapses of the ϵ, β, 4, and 5 rings were in the northern ansa, while the α ring's periapsis was in the south.

The results indicate (Table 6) that the rings (with the exception of the ϵ ring) do not show any significant variation in brightness from north to south except for a possible increase in brightness of the η ring (which is not known to have a simple orbital phase variation in brightness). This indicates, first, that our modeling is not compromised by the assumption of a constant ring brightness; and second, that

variations in the widths of the α and β rings (assuming that these widths are the same as those measured by Voyager in 1986) do not lead to variations in ring brightness. One explanation for the lack of variation in brightness is that these rings have a lower optical depth than the ϵ ring; thus there is little particle shadowing and little effect on ring brightness of a widening or narrowing of the ring. Another possibility is that there has been a change in ring width since the occultation measurements were made. Further observations are obviously needed to clarify this point.

5. Conclusions

Our observations of the uranian satellite and ring system at near-infrared wavelengths have produced the first resolved images of individual faint rings of Uranus. We have presented values for the albedo of uranian satellites in broadband J, H, and Kp filters which are in good agreement with previous values, and confirm the opposition surge found by Karkoschka (2001a).

Our values for the ring group reflectivities are in excellent agreement with previous measurements (de Pater et al., 2002; Karkoschka, 2001a). We find the ring albedo to be quite flat in the range from 1.17 to 2.3 µm. However, the equivalent depths for individual rings are found to be different from previous values (French et al., 1986), if we assume that all the ring particles in the uranian system have the same brightness.

We find a value of 3.2 for the north/south brightness ratio of the ϵ ring (which is close to the apoapse/periapse ratio q), in good agreement with the Karkoschka (2001b) model with a filling factor of 0.06. For the α and β rings q is close to 1.0, which indicates no significant brightness difference despite an orbital phase variation in ring width. This suggests either that there is relatively little shadowing occurring in these rings, or perhaps that the periapse/apoapse width variation has changed in time. Further observations, especially as Uranus approaches ring plane crossing in 2007 with an expected large increase in q, will help clarify this issue.

References

Baines, K.H., Yanamandra-Fisher, P.A., Lebofsky, L.A., Momary, T.W., Golish, W., Kaminski, C., Wild, W.J., 1998. Near-infrared absolute photometric imaging of the uranian system. Icarus 132, 266–284.

Brown, R.H., Cruikshank, D.P., 1983. The uranian satellites: surface compositions and opposition brightness surges. Icarus 55, 83–92.

de Pater, I., Gibbard, S.G., Macintosh, B.A., Roe, H.G., Gavel, D.T., Max, C.E., 2002. Keck adaptive optics images of Uranus and its rings. Icarus 160, 359–374.

Dones, L., Cuzzi, J.N., Showalter, M.R., 1993. Voyager photometry of Saturn's A ring. Icarus 105, 184–215.

French, R.G., Elliot, J.L., Levine, S.E., 1986. Structure of the uranian rings. II. Ring orbits and widths. Icarus 67, 134–163.

French, R.G., Nicholson, P.D., Porco, C.C., Marouf, E.A., 1991. Dynamics and structure of the uranian rings. In: Bergstrahl, J.T., Miner, E.D., Matthews, M.S. (Eds.), Uranus. Univ. of Arizona Press, Tucson, AZ, pp. 327–409.

Hammel, H.B., Rages, K., Lockwood, G.W., Karkoschka, E., de Pater, I., 2001. New measurements of the winds of Uranus. Icarus 153, 229–235.

Hammel, H.B., de Pater, I., Gibbard, S.G., Lockwood, G.W., Rages, K., 2004. Uranus in 2003: zonal winds, banded structure, and discrete features. Icarus. Submitted for publication.

Hapke, B., 1981. Bidirectional reflectance spectroscopy. 1. Theory. J. Geophys. Res. 86, 4571–4586.

Irvine, W.M., 1966. The shadowing effect in diffuse reflection. J. Geophys. Res. 71, 2931–2937.

Karkoschka, E., 1998. Clouds of high contrast on Uranus. Science 280, 570–572.

Karkoschka, E., 2001a. Comprehensive photometry of the rings and 16 satellites of Uranus with the Hubble Space Telescope. Icarus 151, 51–68.

Karkoschka, E., 2001b. Photometric modeling of the epsilon ring of Uranus and its spacing of particles. Icarus 151, 78–83.

Porco, C.C., Goldreich, P., 1987. Shepherding of the uranian rings. I. Kinematics. Astron. J. 93, 724–729.

Press, W.H., Teukolsky, S.A., Vetterling, W.T., Flannery, B.P., 1992. Numerical Recipes in FORTRAN: the Art of Scientific Computing. Cambridge Univ. Press, New York. pp. 402–406.

Smith, B.A., 39 colleagues, 1986. Voyager 2 in the uranian system: imaging science results. Science 233, 43–64.

Sromovsky, L.A., Spencer, J.R., Baines, K.H., Fry, P.M., 2000. Ground-based observations of cloud features on Uranus. Icarus 146, 307–311.

Stone, E.C., Miner, E.D., 1986. The Voyager 2 encounter with the uranian system. Science 233, 39–43.

Svitek, T., Danielson, G.E., 1987. Azimuthal brightness variation and albedo measurements of the uranian rings. J. Geophys. Res. 92, 14979–14986.

van Dam, M.A., Macintosh, B.A., 2003. Characterization of adaptive optics at Keck Observatory. SPIE 5169, 1–10.

van Dam, M.A., Le Mignant, D., Macintosh, B.A., 2004. Performance of the Keck Observatory adaptive optics system. Appl. Optics 43, 5458–5467.